

## VU Research Portal

### Forward ray tracing for image projection prediction and surface reconstruction in the evaluation of corneal topography systems

Snellenburg, J.J.; Braaf, B.; Hermans, E.A.; van der Heijde, R.G.L.; Sicam, V.A.

**published in**

Optics Express  
2010

**DOI (link to publisher)**

[10.1364/OE.18.019324](https://doi.org/10.1364/OE.18.019324)

**document version**

Publisher's PDF, also known as Version of record

[Link to publication in VU Research Portal](#)

**citation for published version (APA)**

Snellenburg, J. J., Braaf, B., Hermans, E. A., van der Heijde, R. G. L., & Sicam, V. A. (2010). Forward ray tracing for image projection prediction and surface reconstruction in the evaluation of corneal topography systems. *Optics Express*, 18(18), 19324-19338. <https://doi.org/10.1364/OE.18.019324>

**General rights**

Copyright and moral rights for the publications made accessible in the public portal are retained by the authors and/or other copyright owners and it is a condition of accessing publications that users recognise and abide by the legal requirements associated with these rights.

- Users may download and print one copy of any publication from the public portal for the purpose of private study or research.
- You may not further distribute the material or use it for any profit-making activity or commercial gain
- You may freely distribute the URL identifying the publication in the public portal ?

**Take down policy**

If you believe that this document breaches copyright please contact us providing details, and we will remove access to the work immediately and investigate your claim.

**E-mail address:**

[vuresearchportal.ub@vu.nl](mailto:vuresearchportal.ub@vu.nl)

# Forward ray tracing for image projection prediction and surface reconstruction in the evaluation of corneal topography systems

Joris J. Snellenburg,<sup>1,\*</sup> Boy Braaf,<sup>2</sup> Erik A. Hermans,<sup>3</sup>  
Rob G.L. van der Heijde,<sup>3</sup> and Victor Arni D. P. Sicam<sup>2,3,4</sup>

<sup>1</sup>Department of Physics and Astronomy, VU University Amsterdam, De Boelelaan 1081,  
1081 HV Amsterdam, The Netherlands

<sup>2</sup>Rotterdam Ophthalmic Institute, Schiedamse Vest 160, 3011 BH Rotterdam, The Netherlands

<sup>3</sup>Department of Physics and Medical Technology, VU University Medical Center, De Boelelaan 1118,  
1081 HZ Amsterdam, The Netherlands

<sup>4</sup>i-Optics BV, Westeinde 12C, 2512 HD The Hague, The Netherlands

\*j.snellenburg@few.vu.nl

**Abstract:** A forward ray tracing (FRT) model is presented to determine the exact image projection in a general corneal topography system. Consequently, the skew ray error in Placido-based topography is demonstrated. A quantitative analysis comparing FRT-based algorithms and Placido-based algorithms in reconstructing the front surface of the cornea shows that arc step algorithms are more sensitive to noise (imprecise). Furthermore, they are less accurate in determining corneal aberrations particularly the quadrafoil aberration. On the other hand, FRT-based algorithms are more accurate and more precise showing that point to point corneal topography is superior compared to its Placido-based counterpart.

©2010 Optical Society of America

**OCIS codes:** 170.4460 (Ophthalmic Optics and Devices); 220.1010 (Aberrations (Global)); 080.1753 (Computation Methods); 170.4470 (Ophthalmology)

---

## References and links

1. J. Amanatides, "Ray tracing with cones," *Comput. Graph.* **18**(3), 129–135 (1984).
2. C. Bauer, "Direct illuminance caching: a way to enhance the performance of RADIANCE," *Lighting Res. Tech.* **34**(4), 333–345 (2002).
3. V. A. Sicam, J. J. Snellenburg, R. G. van der Heijde, and I. H. van Stokkum, "Pseudo forward ray-tracing: a new method for surface validation in cornea topography," *Optom. Vis. Sci.* **84**(9), 915–923 (2007).
4. J. D. Doss, R. L. Hutson, J. J. Rowsey, and D. R. Brown, "Method for calculation of corneal profile and power distribution," *Arch. Ophthalmol.* **99**(7), 1261–1265 (1981).
5. J. Y. Wang, D. A. Rice, and S. D. Klyce, "A new reconstruction algorithm for improvement of corneal topographical analysis," *Refract. Corneal Surg.* **5**(6), 379–387 (1989).
6. S. A. Klein, "A corneal topography algorithm that produces continuous curvature," *Optom. Vis. Sci.* **69**(11), 829–834 (1992).
7. R. Mattioli, and N. K. Tripoli, "Corneal geometry reconstruction with the Keratron videokeratographer," *Optom. Vis. Sci.* **74**(11), 881–894 (1997).
8. J. Turuwhenua, "An improved low order method for corneal reconstruction," *Optom. Vis. Sci.* **85**(3), 211–217 (2008).
9. N. K. Tripoli, K. L. Cohen, P. Obla, J. M. Coggins, and D. E. Holmgren, "Height measurement of astigmatic test surfaces by a keratoscope that uses plane geometry surface reconstruction," *Am. J. Ophthalmol.* **121**(6), 668–676 (1996).
10. S. A. Klein, "Axial curvature and the skew ray error in corneal topography," *Optom. Vis. Sci.* **74**(11), 931–944 (1997).
11. S. A. Klein, "Corneal topography reconstruction algorithm that avoids the skew ray ambiguity and the skew ray error," *Optom. Vis. Sci.* **74**(11), 945–962 (1997).
12. F. M. Vos, R. G. L. van der Heijde, H. J. W. Spoelder, I. H. M. van Stokkum, and F. C. A. Groen, "A New Instrument to Measure the Shape of the Cornea Based on Pseudorandom Color Coding," *IEEE Trans. Instrum. Meas.* **46**(4), 794–797 (1997).
13. T. Swartz, L. Marten, and M. Wang, "Measuring the cornea: the latest developments in corneal topography," *Curr. Opin. Ophthalmol.* **18**(4), 325–333 (2007).

14. J. H. Massig, E. Lingelbach, and B. Lingelbach, "Videokeratoscope for accurate and detailed measurement of the cornea surface," *Appl. Opt.* **44**(12), 2281–2287 (2005).
15. Y. Mejia, and J. C. Galeano, "Corneal topographer based on the Hartmann test," *Optom. Vis. Sci.* **86**(4), 370–381 (2009).
16. M. A. Halstead, B. A. Barsky, S. A. Klein, and R. B. Mandell, "A spline surface algorithm for reconstruction of corneal topography from a videokeratographic reflection pattern," *Optom. Vis. Sci.* **72**(11), 821–827 (1995).
17. V. A. Sicam, J. Coppens, T. J. van den Berg, and R. G. van der Heijde, "Corneal surface reconstruction algorithm that uses Zernike polynomial representation," *J. Opt. Soc. Am. A* **21**(7), 1300–1306 (2004).
18. J. Turuwhenua, "Corneal surface reconstruction algorithm using Zernike polynomial representation: improvements," *J. Opt. Soc. Am. A* **24**(6), 1551–1561 (2007).
19. V. A. Sicam, and R. G. VAN der Heijde, "Topographer reconstruction of the nonrotation-symmetric anterior corneal surface features," *Optom. Vis. Sci.* **83**(12), 910–918 (2006).
20. V. Sokurenko, and V. Molebny, "Damped least-squares approach for point-source corneal topography," *Ophthalmic Physiol. Opt.* **29**(3), 330–337 (2009).
21. L. A. Carvalho, "Accuracy of Zernike polynomials in characterizing optical aberrations and the corneal surface of the eye," *Invest. Ophthalmol. Vis. Sci.* **46**(6), 1915–1926 (2005).
22. Matlab, The Mathworks, Massachusetts, USA.
23. R. H. Rand, H. C. Howland, and R. A. Applegate, "Mathematical model of a Placido disk keratometer and its implications for recovery of corneal topography," *Optom. Vis. Sci.* **74**(11), 926–930 (1997).
24. S. Marcos, P. Rosales, L. Llorente, and I. Jiménez-Alfaro, "Change in corneal aberrations after cataract surgery with 2 types of aspherical intraocular lenses," *J. Cataract Refract. Surg.* **33**(2), 217–226 (2007).
25. O. Muftuoglu, P. Prasher, R. W. Bowman, J. P. McCulley, and V. V. Mootha, "Corneal higher-order aberrations after Descemet's stripping automated endothelial keratoplasty," *Ophthalmology* **117**(5), 878–884, e6 (2010).
26. L. N. Thibos, X. Hong, A. Bradley, and X. Cheng, "Statistical variation of aberration structure and image quality in a normal population of healthy eyes," *J. Opt. Soc. Am. A* **19**(12), 2329–2348 (2002).
27. L. A. Carvalho, M. Stefani, A. C. Romão, L. Carvalho, J. C. de Castro, S. Tonissi, P. Schor, and W. Chamon, "Videokeratoscopes for dioptric power measurement during surgery," *J. Cataract Refract. Surg.* **28**(11), 2006–2016 (2002).
28. F. Lu, J. X. Wu, J. Qu, *et al.*, "Association between offset of the pupil center from the corneal vertex and wavefront aberration," *J. Opt.* **1**, 8–13 (2008).
29. T. O. Salmon, and L. N. Thibos, "Videokeratoscope-line-of-sight misalignment and its effect on measurements of corneal and internal ocular aberrations," *J. Opt. Soc. Am. A* **19**(4), 657–669 (2002).
30. R. A. Applegate, J. D. Marsack, and L. N. Thibos, "Metrics of retinal image quality predict visual performance in eyes with 20/17 or better visual acuity," *Optom. Vis. Sci.* **83**(9), 635–640 (2006).
31. B. Braaf, M. Dubbelman, R. G. van der Heijde, and V. A. Sicam, "Performance in specular reflection and slit-imaging corneal topography," *Optom. Vis. Sci.* **86**(5), 467–475 (2009).

## 1. Introduction

Ray tracing is a powerful technique to predict outcomes of wave propagation. The forward approach is a natural, logical method where propagation is traced from the source to other points of interest. For example, forward ray tracing (FRT) simulation has been used in rendering, where images are synthesized from a model by means of computer programs [1]. Unfortunately, the forward approach is computationally expensive and in most cases impractical. The backward approach (backward ray tracing) where rays are traced back from the image to the source is often used instead of the forward approach [2]. Nevertheless, clever use of backward ray tracing can simulate forward ray tracing: i.e. multidirectional ray tracing in lighting analysis and pseudo forward ray tracing in corneal topography [2,3]. There are no known forward ray tracing algorithms applied in corneal topography (CT) because it is difficult to predict which among the infinite directions from the light source will propagate towards its appropriate image location. However in this paper, it is demonstrated that with proper modeling of a specular reflection CT system, corneal reflection images can be accurately determined using forward ray tracing.

A widely used CT system uses a technique in which a Placido ring source is used. Current surface reconstruction algorithms used in combination with this technique use iterative procedures such as arc step algorithms. Arc step algorithms are an implementation of backward ray tracing along a surface which is assumed to be continuous and composed of a series of arcs. Early algorithms were developed by Doss *et al.* [4] and Wang *et al.* [5]. These algorithms were further improved throughout the years [6–8]. A major issue that was addressed is the skew ray error in the surface reconstruction of Placido-based systems [8–10].

The skew ray error arises because of the assumption that the tracing of the light from the image to the source happens within a meridional plane. This is only applicable for rotationally symmetric surfaces, which is not the case for the cornea. Therefore, errors in the corneal height reconstruction occur and are aptly called skew ray errors. This problem was first mentioned by Tripoli [9] and methods were thought of to solve this [10–12]. One approach was to stick to the Placido-based system and develop appropriate surface reconstruction algorithms that would correct for skew-ray errors. Klein proposed such an algorithm in 1997 [11] but this method does not appear to have been implemented in any commercial topographer [13].

Another approach to solve the skew ray error problem is to move away from the Placido-based systems and introduce alternate stimulator designs which provide one-to-one correspondence between image points and source points [12–15]. This allows for corneal surface reconstruction algorithms which include skew rays and thus are free from skew-ray errors [16–18]. This approach has preliminary validation on artificial surfaces and eyes and was shown to be at least as accurate in reconstructing rotationally symmetric features of the cornea as Placido-based methods but more accurate in reconstructing non-rotationally symmetric corneal surface features [19]. This was also demonstrated by computer simulations for a telecentric CT system which include noise analysis [20].

To further strengthen the proof that topographers allowing for one-to-one correspondence of image and source points are superior to Placido-based systems, a new algorithm for surface reconstruction based on the principle of forward ray tracing is introduced. This algorithm is validated and compared with existing arc step based algorithms in reconstructing simulated surfaces in which the accuracy and precision of the algorithms is evaluated under different noise conditions. Simulation of a nodal point CT system was chosen for comparison and typical parameter values were assigned based on an existing experimental topographer [3,19]

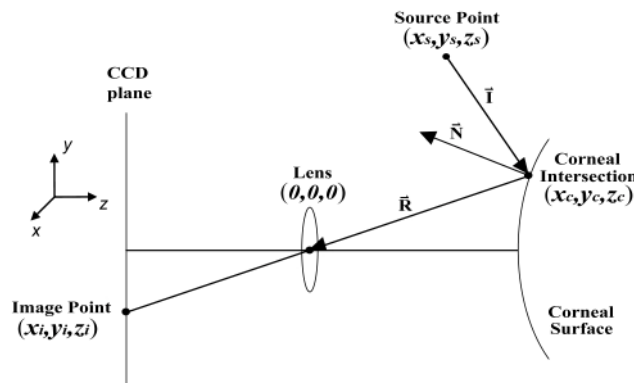


Fig. 1. Diagram of forward ray tracing model

## 2. The FRT model for nodal point CT systems

The corneal surface produces distinguishable specular reflections for appropriate light sources. In modeling the reflection phenomenon for a CT system (see Fig. 1) the light sources are modeled as source points (x<sub>s</sub>, y<sub>s</sub>, z<sub>s</sub>). These are traced towards the intersection points on the corneal surface (x<sub>c</sub>, y<sub>c</sub>, z<sub>c</sub>) and proceed with the reflected ray towards the image points (x<sub>i</sub>, y<sub>i</sub>, z<sub>i</sub>) captured by a camera. Because only the chief ray is considered the reflected ray is constrained to pass through the nodal point (0, 0, 0) of the camera lens system. These definitions are summarized in Table 1. A telecentric system can also be employed instead of the nodal point system described here, by adequately modifying the nodal-point constraint. It

is known that surface reconstruction for both systems are quite similar and are described well in literature [8].

The goal of forward ray tracing is to be able to determine the image points, when the source points and the corneal surface shape are known. The corneal surface, the incident vector and the reflected vector can easily be represented by simple equations (Eqs. (1-3) in Table 1). Here  $f(x_c, y_c)$  in Eq. (1) represents a function composed of Zernike polynomials parameterized by Zernike polynomial coefficients evaluated over an 6 mm corneal zone. A Zernike polynomials expansion is an appropriate way of expressing the corneal surface [17,18]. It should be noted that Zernike representation can describe any corneal surface as long as sufficient number of coefficients is used [3,21]. For this reason, order 8 (45 terms) was chosen to describe surfaces considered in this paper. Only the octafoil surface described later in this paper will have a better description when the Zernike order is increased but for the purpose of preliminary analysis we start with order 8. Equation (2) and 3 represent the incident and reflected vectors respectively and are determined from the normal vector  $N$  on the corneal surface. The normal vector  $N$  is derived by taking the surface gradient using the partial derivatives of Eq. (1) and is given by Eq. (6). The relation the corneal normal describes with the incident unit vector  $I$  and the reflected vector  $R$  is captured by Eqs. (4) and 5. Equation (4) constrains the direction of the surface normal to be in the same direction of the angle bisector of the incident and reflected ray while Eq. (5) places the normal vector to lie in the same plane as the incident and reflected ray. Equations (1-5) are actually 11 scalar equations containing 11 unknowns:  $x_c, y_c, z_c, I_x, I_y, I_z, R_x, R_y, R_z, l_I, l_R$ , where  $I_x, I_y, I_z, R_x, R_y, R_z$  and  $l_I, l_R$  are the directional cosines and the lengths of the incident and reflected vectors respectively. Note that Eqs. (2), 3 and 5 are vector equations which can be decomposed into

**Table 1. Definitions and equations for the forward ray tracing model**

Description		Equation
Reflection source point		$(x_s, y_s, z_s)$
Reflection image point		$(x_i, y_i, z_i)$
Intersection point on the cornea		$(x_c, y_c, z_c)$
Incident vector (length x directional cosines)		$\ell_I \langle I_x, I_y, I_z \rangle$
Reflected vector (length x directional cosines)		$\ell_R \langle R_x, R_y, R_z \rangle$
Normal vector $\vec{N}$ on the corneal surface		$\langle N_x, N_y, N_z \rangle$
Equation of the surface	$-z_c + f(x_c, y_c) = 0$	(1)
Incident Vector	$\langle x_c - x_s, y_c - y_s, z_c - z_s \rangle = \ell_I \langle I_x, I_y, I_z \rangle$	(2)
Reflected Vector	$\langle -x_c, -y_c, -z_c \rangle = \ell_R \langle R_x, R_y, R_z \rangle$	(3)
Dot Product	$(\vec{I} + \vec{R}) \bullet \vec{N} = 0$	(4)
Cross Product	$(\vec{I} - \vec{R}) \times \vec{N} = 0$	(5)
Surface Gradient	$\langle N_x, N_y, N_z \rangle = \left\langle \frac{\partial f}{\partial x_c}, \frac{\partial f}{\partial y_c}, -1 \right\rangle$	(6)

three scalar equations each, however the dot product equation (Eq. (4)) results into only one scalar equation. This balanced set of equations and unknowns makes it possible to determine the solution of the corneal intersection points  $x_c$ ,  $y_c$  and  $z_c$  by standard mathematical software (e.g. using the *fsolve* routine in Matlab [22]). Consequently, the location of the image points captured by the camera can be determined by direct ray tracing from the corneal intersection points to the nodal point of the lens and further to the camera plane.

### 3. Surface reconstruction method derived from FRT

Using the FRT algorithm, a direct tracing from source points via a known surface to the image plane can be done, thus directly simulating the image points. This is a powerful validation technique which is an upgrade of an earlier development, the pseudo forward ray tracing (PFRT) algorithm [3]. The PFRT simulates forward ray tracing by evaluating a bundle of back-traced rays from the neighborhood of image points. The FRT on the other hand uses only the chief ray and thus is less computationally expensive.

A further use of the FRT algorithm can be made by applying the same principles in corneal surface reconstruction. Given, a set of known source points and corresponding image points the corneal surface can be reconstructed using a similar set of equations to that described in Table 1. Equation (3) is now modified into:

$$\langle x_i, y_i, z_i \rangle = \ell_R \langle R_x, R_y, R_z \rangle \quad (7)$$

This is derived by tracing from the nodal point to the image point. All parameters in Eq. (7) are now known variables. By combining Eq. (7) with the Eqs. (1-6), an iterative solution to find the appropriate Zernike coefficients describing the corneal surface can be determined using a step by step procedure. The procedure which is similar to an earlier method [17] is described as follows:

**STEP 1:** Create matrix equations derived from the equations in Table 1 and Eq. (7):

$$\frac{z_c}{r_p} = M \left( \frac{x_c}{r_p}, \frac{y_c}{r_p} \right) \mathbf{C} \quad (8)$$

This is the surface equation expressed in Zernike convention:  $r_p$  is the pupil radius used as a reference for a unit circle,  $M$  is the matrix representation of the Zernike polynomials and  $\mathbf{C}$  represents the Zernike coefficients. Finally, we have two matrix equations from the cross product (Eq. (5)):

$$I_x - R_x = -(I_z - R_z) \frac{\partial M}{\partial x} \mathbf{C} \quad (9)$$

$$I_y - R_y = -(I_z - R_z) \frac{\partial M}{\partial y} \mathbf{C} \quad (10)$$

**STEP 2:** Use zero initial values for the Zernike coefficients to represent a flat surface in the corneal apex plane. Via ray tracing, image points can be traced to the apex plane and form the points  $(x_c, y_c, z_c)$ .

**STEP 3:** Use  $(x_c, y_c, z_c)$  as information to calculate a new set of Zernike coefficients  $\mathbf{C}$  by exploiting the matrix Eqs. (8-10). These matrix equations can be cast into the form:

$$A(x_c, y_c, z_c) = B(x_c, y_c, z_c) \mathbf{C} \quad (11)$$

The solution for Eq. (11) is given by:

$$\mathbf{C} = [\mathbf{B}^T \mathbf{B}]^{-1} [\mathbf{B}^T \mathbf{A}] \quad (12)$$

Which can be solved numerically using the Moore-Penrose pseudo inverse algorithm.

**STEP 4:** Go back to STEP 2 to build a new surface with the new Zernike coefficients. Proceed to STEP 3 to determine more accurate Zernike coefficients. Repeat this iteration until a desired accuracy has been reached.

The convergence of the outlined procedure is quite fast. With three iterations sub-micron accuracy can already be achieved.

## 4. Simulation of corneal topography systems

### 4.1 Qualitative evaluation

The forward ray tracing model described above can now be used to illustrate the skew ray error problem encountered in Placido-based corneal topography [9,10,19,23]. Figure 2 describes forward ray traced simulated Placido reflection pattern of a 6 Diopter toric surface (Fig. 2a) and the Rand surface (Fig. 2c) with 8 mm base radius. The Rand surface is a hypothetical surface that was used to simulate a radially keratotomized eye [23]. It is a surface characterized by a smooth spherical surface within the 3 mm central corneal zone and an octafoil corrugation on the periphery. 20 rings are considered within an 8 mm corneal zone. Each ring is traced from 256 meridian source points. The two red circle outlines correspond to the reflection of the 10th and 20th ring on a sphere with 8 mm radius. The reflection pattern in Fig. 2c is quite similar to an experimental photo of an actual artificial Rand surface (Fig. 4 in ref [19]). In an actual Placido reflection only a continuous ring pattern is observed and not the density distribution of points within the ring as revealed by the FRT simulation. Figure 2b and Fig. 2d show another description of Fig. 2a and Fig. 2c only this time limiting the tracing of rays to 8 meridians. Red circles are image points on the meridian and Blue squares are the actual forward ray traced image points. Because the surface reconstruction in Placido-based system is limited to meridional ray tracing, taking the Red circles instead of the Blue squares as actual input for the surface reconstruction produces the so called “skew ray error”.

Although the skew ray error problem has been known for quite some time, motivation to correct this problem was initially not strong because the effect of this problem does not have a large impact when evaluating corneal curvature, astigmatism and asphericity, which are standard parameters used in the clinical practice [9]. However, due to recent developments in ophthalmic optics, particularly in customized laser refractive surgery procedures, the importance of being able to measure other higher order aberrations such as coma, trefoil, quadrafoil and spherical aberration has become apparent. A recent study found that astigmatism, trefoil and quadrafoil aberration was induced by cataract surgery using superior incision [24] emphasizing the importance to measure this aberration accurately to identify the impact of different incision strategies in cataract surgery.

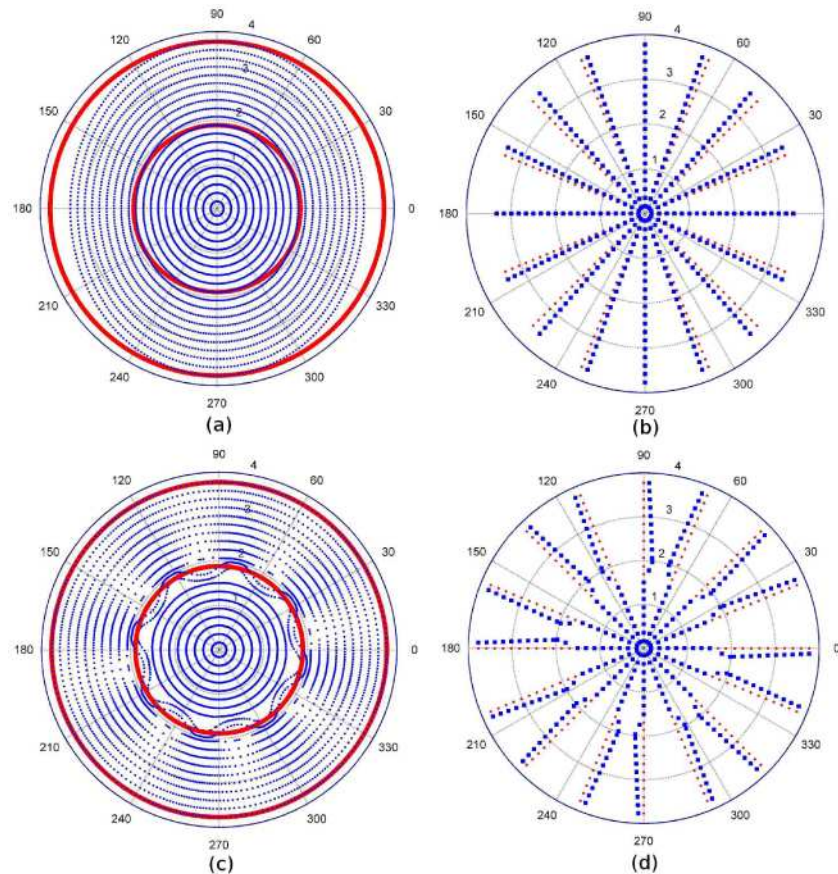


Fig. 2. Illustration of skew ray error in Placido-based corneal topography. Depicted are the forward ray traced simulated Placido reflection patterns of a 6 Diopter toric surface (a,b) and the Rand surface (c,d) with 8 mm base radius. The surfaces are evaluated in an 8mm corneal region for 20 rings with either 256 meridians (a,c) or 8 meridians (b,d). The two red circle outlines corresponds to the reflection of the 10th and 20th ring on a sphere with 8 mm radius. Red dots are image points on the meridian and blue squares are the actual forward ray traced image points.

#### 4.2 Quantitative evaluation

For a quantitative evaluation of the effect of skew ray error in corneal topography four different algorithms were used to reconstruct simulated artificial and corneal surfaces:

- 1) FRT-based surface reconstruction algorithm (FRT algorithm) described in section 3.
- 2) FRT-based surface reconstruction algorithm with meridional constraint (MRT algorithm). This means that the tracing of rays from the image points to the source points is constrained to lie on the same meridian. This algorithm will show the effect of neglecting skew ray errors entirely.
- 3) Basic arc step algorithm (Basic AS algorithm) described in ref [6]. The arc step algorithm does calculations on a per meridian basis. The algorithm tries to converge to calculated corneal height values by assuming that the corneal surface is spherical on a local scope and therefore considers a set of intersections of light rays on the cornea. Adjacent points within one meridian should form an arc and the algorithm makes sure that the connections between consecutive arcs are continuous, in other words the derivatives at the arc boundaries match.



- 4) Arc step algorithm with skew ray error correction (SKEC AS algorithm) described in ref [8]. For this study, the implementation is done for a nodal point system as described in Fig. 1 instead of the original implementation in a telecentric system as described in literature.

The performance of corneal surface reconstruction algorithms is dependent on a large number of variables: the number of detected points, the accuracy of the point or edge detection algorithms, the amount of noise in the system, and the calibration accuracy, to name a few. In order to make a good comparison between various reconstruction algorithms it is important to ensure the simulated experimental conditions are similar. In this study the following experimental conditions were taken into account:

- Identical stimulator pattern for all algorithms; the typical square one-to-one stimulator design was modified to match a Placido disk based design. However, where the one-to-one correspondence algorithm had full information on the location of the detected points, for the arc step algorithms only the information on the meridians was made available.
- An equal number of data points available to both algorithms, equal to the number of rings times the number of meridians.
- Equal noise amplitude applied; however due to the nature of the difference between Placido disk systems and one-to-one systems the effect of the applied noise varies slightly. The implementation of the noise is described more precisely in the later part of this section.

The following surfaces are simulated:

- 1) A toric surface with 8.0 mm and 7.5 mm maximum and minimum meridional radius of curvature; both meridional axes are perpendicular to each other.
- 2) A spherical surface of 8mm radius of curvature with trefoil aberration.
- 3) A spherical surface of 8mm radius of curvature with quadrafoil aberration.
- 4) A spherical surface of 8mm radius of curvature with octafoil aberration.
- 5) A typical corneal surface without abnormalities.

Surfaces 2-4 are multi-foil surfaces that are in the same class of a surface type first described by Rand et al. [23]. These surfaces can be described in cylindrical coordinates ( $\rho, \theta, z$ ) where the corneal sag,  $z$ , is:

$$z = r - \sqrt{r^2 - \rho^2} + g(\rho, \theta) \quad (13)$$

Where  $g$  represents the deviation from a sphere of radius  $\rho$  and is given by:

$$g(\rho, \theta) = \begin{cases} \varepsilon \sin(n\theta) & \text{for } \rho \geq 2\text{ mm} \\ 2(\rho - 1.5)\varepsilon \sin(n\theta) & \text{for } 1.5 < \rho < 2\text{ mm} \\ 0 & \text{for } \rho \leq 1.5\text{ mm} \end{cases} \quad (14)$$

Here  $\varepsilon$  is the amplitude of the peripheral corrugation on the surface (for the simulation this was set to 0.01 mm),  $r$  is the surface base radius of curvature set at 8 mm,  $n = 3, 4, 8$  for trefoil, quadrafoil and octafoil respectively.

Surface 5 is a simulation of a real corneal surface. Corneal aberrations for this eye were chosen based on the data from ref [25]. Data from the study is available up to Zernike radial order 6 so the coefficients for order 7 and order 8 are assigned zero values. The root mean square (rms) values of the relevant Zernike coefficients representing various corneal aberrations are summarized in Table 2 below.

**Table 2. Corneal aberration of a simulated surface of a real cornea**

Corneal Aberration ( $\mu\text{m}$ )	rms up to order 8
Spherical	1.434
Astigmatism	0.750
Coma	0.418
Trefoil	0.172
Quadrafoil	0.181

Each simulated surface is used as a reference to calculate the error in surface reconstruction for each algorithm. This error is calculated by the root mean square of the error in the Zernike coefficients representing the reconstructed surface as recovered by the specific algorithm when compared with the simulated surface. The simulated and reconstructed surfaces are represented by Zernike polynomials expansion of up to 8<sup>th</sup> radial order. The stimulator point pattern chosen for the simulation is a dotted ring system (10 rings, 180 points per ring within a 6 mm corneal zone). This allows for a clear comparison between a one-to-one correspondence topography system and a Placido-based topography system. The source points are arbitrarily chosen to be located at a plane 50 mm away from the corneal apex. These points were generated using back ray tracing from the camera plane, where the image pattern forms rings that have equidistant spacing from each other, to an 8 mm radius of curvature spherical surface and to the plane assigned for the source points. The distance between the nodal point of the lens and the corneal apex is chosen to be 105 mm for this simulation. These dimensions roughly correspond with the dimensions of the experimental corneal topography machine described in refs [3,19].

After the source points are generated, the FRT algorithm is used to predict the image points resulting from reflections on the simulated surface. This was done for specific surfaces to generate image points on the camera. The set of source points and image points are used as input for the FRT surface reconstruction algorithm. Because the three other algorithms are tracing light rays along a meridian, the location of the source points are adjusted so that the “new assigned source point” will be located on the same meridian as the image points.

The performances of the four algorithms are first evaluated assuming there is no noise present in the measurement of the image points. The results are summarized in Table 3. In this case the FRT algorithm shows machine accuracy (error  $< 1 \times 10^{-15} \mu\text{m}$ ). The MRT algorithm produced the biggest error, under-estimating the true value by an order of 1  $\mu\text{m}$ . The arc step algorithms produce larger errors compared to the FRT algorithm but the amount of error is clinically not relevant, noting that 1  $\mu\text{m}$  RMS error is equal to 0.77 equivalent Diopter error [26]. For the case of trefoil aberration and astigmatism the SREC AS algorithm reduced the rms error of the basic arc step algorithm. This was not the case for the quadrafoil and octafoil aberration.

**Table 3. Performance of the four algorithms on four artificial surfaces.**  
**The error in  $\mu\text{m}$  of the aberration corresponding to the most dominant feature of the surface is evaluated.**

	RMS of dominant feature	FRT	MRT	Basic AS	SREC AS
RMS astigmatism	3.0984	$< 1 \times 10^{-15}$	1.3794	0.0004	0.0001
RMS trefoil	1.5031	$< 1 \times 10^{-15}$	0.6896	0.0018	-0.0016
RMS quadrafoil	1.5004	$< 1 \times 10^{-15}$	0.8397	0.0034	-0.0107
RMS octafoil	1.7311	$< 1 \times 10^{-15}$	1.1449	-0.0026	-0.2577

Similarly for the simulated corneal surface, compared to the artificial surfaces, the FRT algorithm shows machine accuracy (error  $< 1 \times 10^{-15} \mu\text{m}$ ) in reconstructing the corneal

aberrations. The results are summarized in Table 4. The MRT algorithm shows larger errors in the order of a small fraction of a micrometer.

**Table 4. Performance of the four algorithms on a simulated corneal surface.**  
The error in  $\mu\text{m}$  of the non-rotationally symmetric aberration is evaluated.

	RMS of dominant feature	FRT	MRT	Basic AS	SREC AS
RMS astigmatism	0.7498	$< 1 \times 10^{-15}$	0.0819	-0.0150	0.0008
RMS trefoil	0.1717	$< 1 \times 10^{-15}$	-0.0439	0.0019	0.0030
RMS quadrafoil	0.1808	$< 1 \times 10^{-15}$	-0.0296	0.0017	0.0015

Figure 3 shows residual curvature plots of the different algorithms in reconstructing the simulated corneal surface. The residual curvature is calculated by taking the absolute difference of the curvature map of the simulated surface and the curvature map of the reconstructed surface by the algorithm. The FRT algorithm produced a flat residual curvature map (negligible error). The largest local curvature was produced by the MRT algorithm. The arc step algorithm has an improved performance compared to the MRT algorithm. This performance was further improved by the SREC AS algorithm.

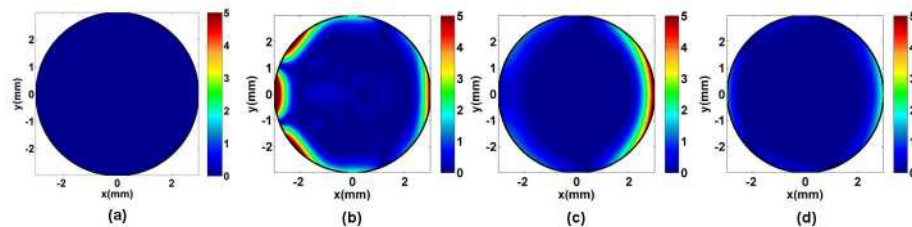


Fig. 3. Residual curvature map in Diopter for a simulated cornea with no abnormalities. Here (a) represents the reconstruction by the FRT algorithm, (b) is the reconstruction by MRT algorithm, (c) is the reconstruction by the Basic AS algorithm and (d) is the SREC AS algorithm.

### 4.3 Effect of noise

So far the quantitative analysis is done without the presence of noise in the system. In actual measurements the presence of noise is inevitable. Many factors contribute to this, i.e. eye movements, shadows created by nose and eye-lashes, pixel resolution of the camera, fluctuations of the light intensity captured by the camera, alignment precision of the instrument to name a few. Noise will have an effect on the performance of corneal surface reconstruction algorithms. This was first mentioned by Klein [11], stating that one-to-one correspondence corneal topography surface reconstruction described by Halstead [16] has greater robustness to noise than arc step algorithms. This was confirmed recently by Sokurenko [20]. We also implemented noise simulation in this study. Gaussian noise was applied to the image points (at a modified camera plane such that there is unit magnification between the camera plane and the corneal apex plane) and the amplitude was varied taking values of 0, 1, 2, 4, 6, 8 and 10  $\mu\text{m}$ . The range from 0 to 10  $\mu\text{m}$  amplitude noise was chosen to account for typical camera resolution of corneal topography systems [19,20,27]. This range is on the conservative side because this does not include effects of eye movements and other factors that contribute to noise. Another important consideration is the fact that for Placido-based corneal topography, the edge detection of the rings has a big effect. For this case, subpixel accuracy can be achieved in the direction along the ring but there would be more uncertainties in the radial direction (perpendicular to the ring) [11,19], therefore the appropriate noise distribution in this case would be radially oriented, as it is applied in this study. For the SREC AS algorithm, only the performance for 0 and 1  $\mu\text{m}$  noise is reported

because the algorithm is unstable for noise  $\geq 2 \mu\text{m}$ . The noise simulation was done for 100 realizations. The performance of the four algorithms were assessed in terms of accuracy (the difference between the mean value of the measurements and the actual value) as represented by the height of the bars in the figures and precision (the spread expressed in standard deviation of the measured values) as represented by the error bars in the figures.

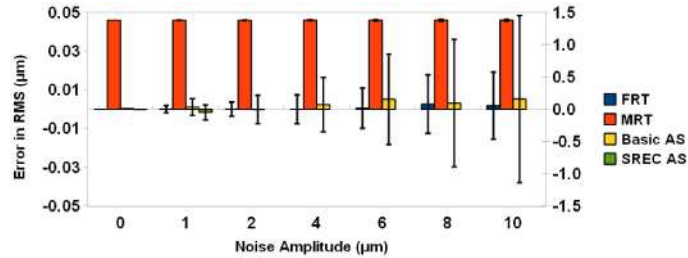


Fig. 4. Astigmatism error in RMS (up to Zernike order 8) of artificial surface. The results for the MRT algorithm are plotted with respect to the secondary y-axis.

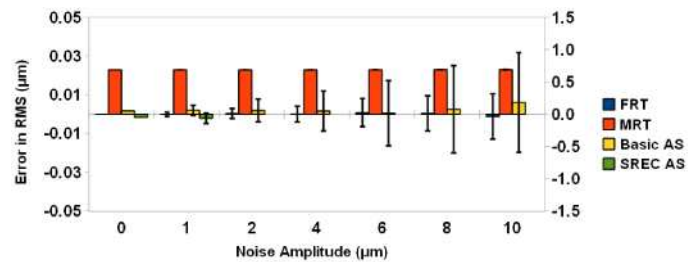


Fig. 5. Trefoil error in RMS (up to Zernike order 8) of artificial surface. The results for the MRT algorithm are plotted with respect to the secondary y-axis.

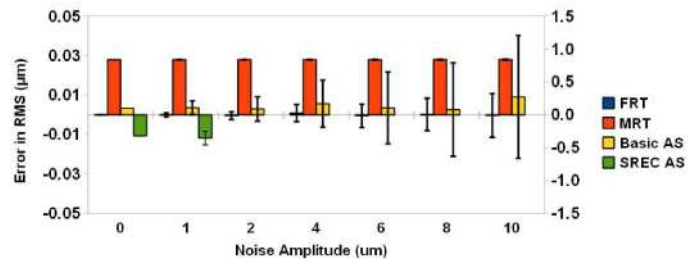


Fig. 6. Quadrafoil error in RMS (up to Zernike order 8) of artificial surface. The results for the MRT algorithm are plotted with respect to the secondary y-axis.

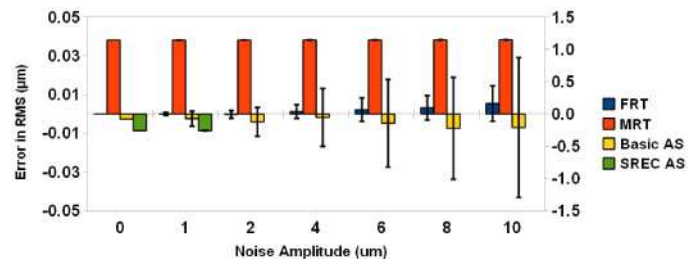


Fig. 7. Octafoil error in RMS (up to Zernike order 8) of artificial surface. The results for the MRT algorithm and the SREC AS algorithm are plotted with respect to the secondary y-axis.

Figure 4-Fig. 7 show the effect of noise in the performances of the different algorithms in reconstructing the toric and multifoil surfaces. The results show a consistent trend that the arc

step algorithms are more affected by noise. The spread in the RMS error values are about 2 times greater for the arc step algorithms than the FRT-based algorithms. Although the MRT algorithm produces the largest error, this algorithm is as robust as the FRT algorithm with respect to noise. The spread due to noise for these two systems are almost equal in magnitude.

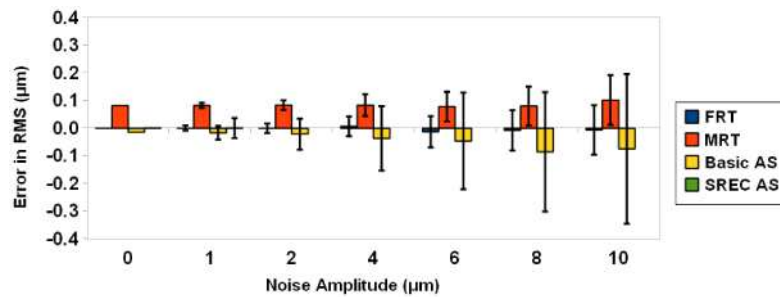


Fig. 8. Astigmatism error in RMS (up to Zernike order 8) of normal eye.

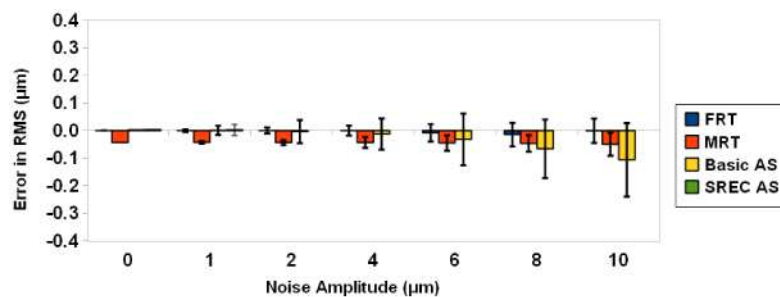


Fig. 9. Trefoil error in RMS (up to Zernike order 8) of normal eye.

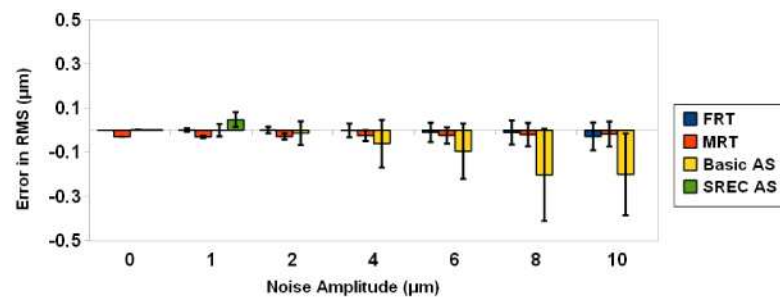


Fig. 10. Quadrafoil RMS error (up to Zernike order 8) of normal eye.

Figure 8-Fig. 10 show the effect of noise in the performances of the different algorithms in reconstructing a typical cornea with no abnormalities. The precision of the arc step algorithms are 2-3 times worse compared to that of the arc step algorithms. Furthermore, as the noise amplitude increases there is also degradation of accuracy for the arc step algorithms. For quadrafoil in particular the accuracy and precision is in the order of quarter of Diopter ( $\sim 0.33 \mu\text{m}$  RMS error).

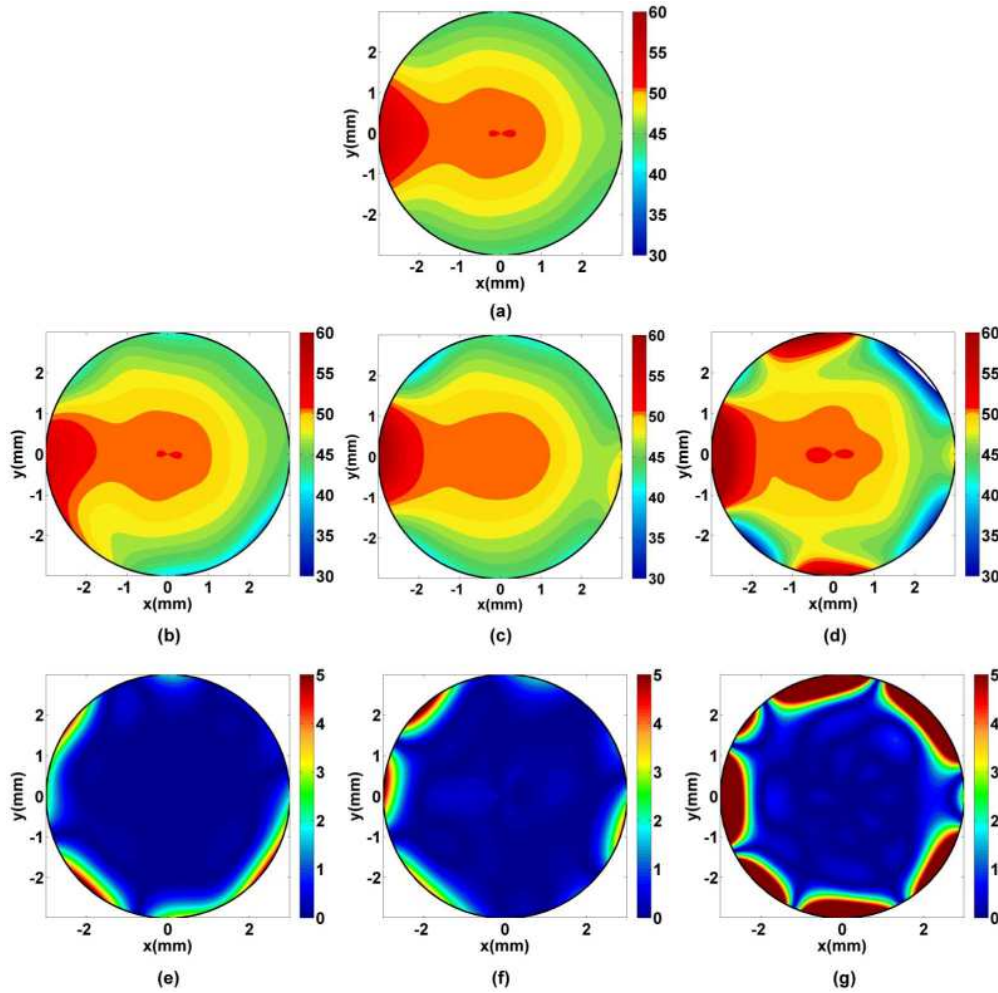


Fig. 11. Curvature maps (a,b,c,d) and residual curvature maps (e,f,g) (in Diopter) of the reconstruction of a cornea with no abnormalities by different algorithms at a noise level of 10 micrometer. The simulated reference surface is represented by (a). The algorithms used for reconstruction are FRT (b,e), MRT (c,f) and Basic AS (d,g). The SKEC AS algorithm was excluded here because of numerical instability at this noise level. The curvature isolines of the curvature maps a,b,c and d are 6/5<sup>th</sup> diopter apart, and the curvature isolines of the residual curvature maps e, f and g are 1/8<sup>th</sup> diopter apart.

As a typical example the curvature maps and corresponding residual curvature maps for a reconstruction of a simulated cornea at a noise level of 10 micrometer are depicted in Fig. 11. The FRT algorithm performs well under these conditions remaining stable well beyond the 4 mm corneal zone region. The MRT algorithm is also relatively stable in the peripheral region but suffers from large artifacts in the central region. The astigmatism as manifested in the bow-tie structure in the actual curvature map disappeared. Finally, the basic arc step algorithm is unstable beyond the 4 mm corneal zone region resulting in residuals of several diopters. Also in the central region some artifacts can be seen in the residual curvature map exceeding 1 diopter appear. The basic arc step curvature map shows an increase magnitude of astigmatism as manifested by the larger bow tie structure. Also, the appearance of a quadrafoil-like artifact is apparent from the orange curvature isolines in Fig. 11d.

## 5. Discussion

In this study the performance of four surface reconstruction algorithms for two types of corneal topography system were evaluated under different experimental conditions, by varying the amount of noise. First the case without any noise is discussed where all experimental conditions are assumed to be perfect and the individual algorithm can be evaluated. It is known that tilt and decentration affect measurements of corneal surfaces [28,29]. However, this aspect was not yet included in the analysis so that a simple and clear description of the effects of skew ray error can be made. The extension of the analysis to include tilt and decentration can be part of future investigations.

### 5.1 Simulations without noise

Out of the four algorithms discussed here, the MRT algorithm is by far the least accurate as can be seen from Table 3, Table 4 and Fig. 3. This demonstrates the danger of not taking into account the skew ray error. On the other hand, the arc step algorithms (Basic AS and SREC AS) are quite accurate in reconstructing the corneal surface. The procedure in arc step algorithms where it is ensured that first and second derivatives are continuous for the whole corneal surface partially corrects for the skew ray error and reduces the error to negligible amounts. It is also notable that the SREC AS algorithm reduces the error of the basic arc step algorithm and this is demonstrated clearly in Fig. 3. However, this does not happen on a consistent basis as can be seen from the reconstruction of the octafoil surface (Table 3) and also the reconstruction of the trefoil component of the simulated cornea (Table 4). We should note that previous demonstrations of the SREC AS algorithm were done in a telecentric CT system while in this study it was implemented in a nodal point system. This could explain why results of previous studies [8,10] were limited to cases where SREC AS algorithm improved the performance of the basic arc step algorithm.

Although the error of the arc step algorithms is small, it is 11-12 orders higher than that of the FRT algorithm. This is consistent with the results of Sokurenko [20] where it was noted that the error of point to point topography was 7-9 orders lower than Placido-based topography. The difference in the order of magnitude observed could be due to differences in the numerical tolerance of the algorithms used, in principle the results show that the accuracy is only limited by the machine precision and noise.

### 5.2 Simulations with noise

There are two notable effects of noise in the performance of corneal surface reconstruction algorithms: the effect in precision and the effect in accuracy.

With regard to precision, the point to point algorithms (FRT and MRT) are least affected by noise compared to their arc step algorithm counterparts. This is true for both artificial surfaces and the simulated corneal surface. The precision of all four algorithms measured for artificial surfaces are quite small ( $< 0.05 \mu\text{m}$ ). The precision measured for the simulated cornea is better than  $0.1 \mu\text{m}$  ( $0.08 \text{ eq D}$ ) for the point to point corneal topography algorithms and can reach as high as  $0.27 \mu\text{m}$  ( $0.21 \text{ eq D}$ ) for the basic arc step algorithm. If we take  $0.125 \text{ diopter}$  as a threshold for clinical relevance [30,31], then we see that the precision of the point to point algorithms even at a noise amplitude of  $10 \mu\text{m}$  is still tolerable while that of the basic arc step algorithm is clinically relevant. It appears that noise interferes with the inherent skew ray error correction mechanism of arc step algorithms. The effect is so great in the SREC AS algorithm that at a noise level of  $2 \mu\text{m}$  the algorithm is already unstable. The SREC AS algorithm [8,11] attempts to improve upon the earlier published arc step algorithms [6] by ensuring that the second derivative, both in radial (along the meridian) and angular (along the ring) direction, is continuous. The results suggest that this will work with no noise in the measurements. In reality, because noise is always present in measurements the performance of the SREC AS algorithm seems to deteriorate quickly which makes it likely

that the algorithm crashes even at a 2  $\mu\text{m}$  noise level. There is also disparity between the precision obtained from artificial surfaces compared to the simulated cornea. This suggests that a good performance in measurement of artificial surfaces does not guarantee a good performance for real corneal surfaces.

In terms of accuracy the FRT algorithm still gives a good performance for all cases even at 10  $\mu\text{m}$  noise level. The worst accuracy was 0.028  $\mu\text{m}$  (0.022 eq D) in reconstructing the quadrafoil aberration of a simulated corneal surface. On the other hand, the accuracy of the arc step algorithms deteriorated with noise and the magnitude of the inaccuracy becomes greater the more complex the non-rotationally symmetric aberrations become. For the basic arc step algorithm, with increasing aberration complexity (astigmatism, trefoil, quadrafoil) the absolute accuracy at 10  $\mu\text{m}$  noise level was 0.075  $\mu\text{m}$  (0.058 eq D), 0.106  $\mu\text{m}$  (0.082 eq D), 0.200  $\mu\text{m}$  (0.154 eq D) respectively. The error in quadrafoil aberration is higher than the clinically tolerable level of 0.125 D and therefore clinically relevant. It is also notable that although the MRT algorithm is inaccurate without noise, the accuracy remains stable in the presence of noise showing that the precision of point to point algorithms is not significantly affected by skew-ray errors.

### 5.3 Clinical implications

It is known that edge artifacts are present in corneal topographic maps when the surface is modeled by Zernike polynomials [3]. Apart from edge artifacts that cover less than 10% of the evaluation area, the residual curvature map of the simulated cornea (see Fig. 11) when FRT is implemented at 10  $\mu\text{m}$  noise level is relatively flat. This is not true for the arc step algorithm. The area of the edge artifact is covering a larger area (about 30%) and the central region does not display a flat residue. There are several patches where the error is greater than 1 Diopter. This will introduce confusion in interpreting corneal curvature maps.

Another important consideration in the clinical set-up is the clinically relevant inaccuracy of Placido-based corneal topography in determining the quadrafoil aberration. This could lead to false diagnosis such as ruling out the corneal shape as a cause of low vision after corneal topography measurements reveal low quadrafoil aberration in cases where the actual quadrafoil aberration is high. Point to point topography will avoid these situations.

## 6. Conclusion

In this paper we developed a forward ray tracing algorithm that can be used for image projection prediction and surface reconstruction in corneal topography. Consequently, it enabled the evaluation of four surface reconstruction algorithms. Two different versions of the arc step algorithm used in Placido-based corneal topography were compared to two algorithms based on the principle of forward ray tracing. It has been demonstrated that the performance of algorithms that use one-to-one correspondence of source and image points are superior to algorithms using meridional constraints even with improved features such as skew ray error correction. When no noise is present, we note that the first order correction to the skew ray error of the basic arc step algorithm gives reasonable results. The arc step algorithm with skew ray error correction performs slightly better, but not in all cases. However when noise is present the arc step algorithms are demonstrably less precise and less accurate than their one-to-one correspondence counterparts. They are inaccurate particularly in determining the correct quadrafoil aberration of the cornea. The FRT algorithm is highly accurate and very robust in all cases and should therefore be preferred over arc step based algorithms.

## Acknowledgements

The authors would like to thank Jason Turuwhenua from the Faculty of Science, University of Auckland, Auckland, New Zealand for providing them with an implementation of the arc step algorithm with skew ray error correction.